Applied Thermal Engineering 232 (2023) 121094

Contents lists available at ScienceDirect

Applied Thermal Engineering

journal homepage: www.elsevier.com/locate/apthermeng

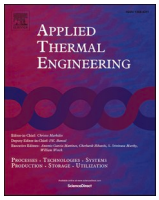

Research Paper

Performance assessment of a novel solar heliostat and digester-based multigeneration system with hydrogen production

Moslem Sharifishourabi [a,*], Ibrahim Dincer [a], Atef Mohany [a]

[a] Clean Energy Research Laboratory, Faculty of Engineering and Applied Science, Ontario Tech. University, 2000 Simcoe Street North, Oshawa, Ontario L1H 7K4, Canada

ARTICLE INFO

Keywords:
Energy
Exergy
Efficiency
Solar energy
Biodigester
Heliostat field
Hydrogen
Electrolysis

ABSTRACT

Renewable energy sources have the potential to mitigate environmental risks by replacing fossil fuels. The aim of this study is firstly to consider the use of renewable energy sources to develop a new multigeneration system for meeting the energy demands of residential communities; secondly to analyze the presently developed system using mass, energy, entropy and exergy balance equations; and finally to assess the system's performance in terms of energy and exergy efficiencies. The system uniquely employs an ammonia-water-based triple-effect absorption system with other systems, such as an organic Rankine cycle, a Brayton cycle, and a steam turbine Rankine cycle. The Engineering Equation Solver (EES) software package is used to determine the thermodynamic properties and perform the aforementioned thermodynamic analyses through the constructed codes. The results of this study show that the steam Rankine, Brayton and organic Rankine cycles have energy efficiencies of 35.90%, 19.50%, and 11.49%, respectively, while the exergy analysis reveals that the steam Rankine, Brayton and organic Rankine cycles achieve the corresponding exergy efficiencies of 74.30%, 31.68%, and 23.23%, respectively. Additionally, the energetic and exergetic coefficients of performance (COPs) of the absorption cooling system are determined to be 1.60 and 0.32, respectively.

1. Introduction

The pressing issue of climate change demands global cooperation and concerted efforts to find solutions. People around the world increasingly recognize renewable energy as a crucial component in addressing this issue and promoting sustainable development. Until recently, non-renewable energy sources such as coal were commonly used for power generation, resulting in hazards such as CO_2 emissions and environmental concerns [1,2]. Residential buildings represent a high share of overall energy usage for heating, cooling, hot water, and electricity. In this regard, multigeneration systems are capable of supplying these energy demands while using renewable energy, which has a less harmful impact on the environment [3,4]. A multigeneration system produces multiple types of energy outputs from one or a few energy inputs. This paper aims not only to develop a new multigeneration system but also to evaluate it through different properties. A recent version of the Engineering Equation Solver (EES) software package [5] is used to determine the thermodynamic properties. Thermodynamic analyses typically involve energy analysis (through the first law), entropy generation evaluation (through the second law), and exergy analysis (through the second laws) [6,7].

Waste recovery has received increased attention in the past few decades. Karaca and Dincer [8] have proposed a multigeneration system using biomass (waste food) to produce different products such as hydrogen, biomethane, electricity, heating, hot water, and fertilizer.

Various types of refrigeration systems are used in the multigeneration systems. For example, numerous researchers have essentially utilized a single effect absorption system (SEAS). Zhou et al. [9] developed a solar-biogas-based multigeneration system, including a single-effect absorption system. Their results showed that the solar power tower was the most influential component in terms of exergy destruction, and the system achieved an exergy efficiency of 24.34%. Bamisile et al. [10] introduced a multigeneration system that combines concentrated solar photovoltaics and wind turbines with different subsystems, such as a single-effect absorption system. They conducted a thermodynamic analysis, and the results of analyses indicated that the overall energetic efficiency of the system was 48.61%, while the exergetic efficiency was 88.31%. In addition, in some studies double effect absorption system are employed such as studies of Ghasemi et al. [11] and Wang et al. [12]. In these studies, Ghasemi et al. [11] suggested and analyzed a biomass-solar based multigeneration system. The system

* Corresponding author.
E-mail address: moslem.sharifishourabi@ontariotechu.ca (M. Sharifishourabi).

https://doi.org/10.1016/j.applthermaleng.2023.121094
Received 2 April 2023; Received in revised form 16 June 2023; Accepted 29 June 2023
Available online 1 July 2023

Nomenclature

Exd	Exergy Destruction Rate (kW)
ex	Specific Exergy (kJ/kg)
h	Specific Enthalpy (kJ/kg)
HHV	Higher Heating Value (kJ/kg)
LHV	Lower Heating Value (kJ/kg)
$\dot{m}$	Mass Flow Rate (kg/s)
MW	Molar Mass of H_2 (kg/kmol)
P	Pressure (kPa)
$\dot{Q}$	Heat Transfer Rate (kW)
s	Specific Entropy (kJ/kgK)
T	Temperature (K)

Greek Letters

η	Energy Efficiency (%)
ψ	Exergy Efficiency (%)

Acronyms

ABS	Absorber
CCH	Combustion Chamber
COM	Compressor
CON	Condenser
COP	Coefficient of Performance
CT	ORC Turbine
CFWH	Closed Feed Water Heater
CH	Condenser Heat Exchanger
EES	Engineering Equation Solver
Elec	Electrolyzer
En	Energy
EV	Absorption Evaporator
G	Generator
GT	Gas Turbine
HEX	Heat Exchanger
HPST	High Pressure Steam Turbine
HTG	High Temperature Generator
HTH	High Temperature Heat Exchanger
LPST	Low Pressure Steam Turbine
LTG	Low Temperature Generator
LTH	Low Temperature Heat Exchanger
MC	Mixing Chamber
MTG	Medium Temperature Generator
MTH	Medium Temperature Heat Exchanger
ORC	Organic Rankine Cycle
P	Pump
REC	Rectifier
SRC	Steam Rankine Cycle
T	Turbine
TES	Thermal Energy Storage
TEAS	Triple Effect Absorption System

Subscripts

abs	Absorber
avg	Average
conv	Convection
ch	Chemical
cond	Conduction
Dig	Digester
em	Emissivity
insu	Insulation

contained a double effect absorption system, a Rankine cycle, a multi-effect desalination system, a Linde-Hampson cycle, a burner, and a parabolic trough solar collector. The results outlined that the energetic and exergetic efficiencies of the system were found to be 46.8% and 11.2%, respectively. Wang et al. [12] evaluated a combined power heating and cooling system. According to the results, the system was found to have an exergy efficiency of 56% and an energy efficiency of 28%.

Moreover, studies such as studies of Zhang et al. [13] and Sharifishourabi and Arabchadegani [14] triple effect absorption systems are utilized. They analyzed a system consisting of absorption refrigeration and an organic Rankine power cycle. Their study revealed that the energy and exergy efficiencies of the system were influenced by operating parameters. In addition, it was found that, under ideal conditions, the energy performance can reach approximately 0.4889. Sharifishourabi and Arabchadegani [14] designed a multigeneration system that provided cooling, heating, conditioned air, and electricity, with solar energy chosen as the primary source. They conducted energetic, exergetic, and environmental impact analyses. The results showed that when the system generated 428 kW of power, the exergy utilization factor was 0.39. Additionally, they determined the energetic and exergetic efficiencies of the organic Rankine cycle to be 14.4% and 26%, respectively. While they calculated the coefficient of performance (COP) of the absorption system to be 1.34. The studies by [13] and [14] used sodium hydroxide-water and lithium bromide-water as the working fluids, respectively. However, the authors of the current article integrated the designed system with a triple effect absorption system working with ammonia water as the solution.

The main goal of this study is to devise a system that produces various forms of energy for residential communities by utilizing two renewable energy sources: biomass and solar energy. What sets this system apart from previous research is its unique combination of an ammonia-water-based triple-effect absorption system with other systems such as an organic Rankine cycle, a Brayton cycle, and a steam turbine Rankine cycle. In addition to these systems, the developed system also includes a thermal storage system and an electrolyzer. The thermal storage system enables the developed system to operate during periods of insufficient solar radiation, while the electrolyzer converts any surplus electricity produced into hydrogen for further usage. The integration of several energy conversion technologies and energy storage systems makes this system an innovative and promising solution for fulfilling the energy needs of residential communities. The specific objectives of the article are threefold as follows:

- To develop a new multigeneration system for producing heating, hot water, cooling, electricity, and hydrogen.
- To analyze the presently developed system through mass, energy, entropy, and exergy balance equations.
- To assess the system's performance through energy and exergy efficiencies to identify what operating conditions and state properties provide better performance and hence better efficiency.

The second section of this article describes the system. The developed system utilizes green energy sources to supply different demands to a residential community. In the third section, thermodynamics balance equations for the major component are presented. These equations analyze the system through thermodynamics equations and also assess the performance of the system through energy and exergy efficiencies. In the fourth section, the study presents the results and the effect of various parameters on the system efficiency.

2. System description

The configuration of the developed multigeneration system is shown in Fig. 1. The system contains 8 subsystems: solar section, digestion unit, thermal energy storage system (TES), organic Rankine cycle (ORC), Brayton cycle (BC), steam Rankine cycle (SRC), electrolyzer system and triple effect absorption system (TEAS). The developed system employs two energy sources, namely solar energy and energy from plant waste. Additionally, the thermal storage system is capable of preserving energy to be used during times of insufficient solar energy or when the system requires more energy. Furthermore, the SRC can generate both electricity and heating that can be distributed to the residential building, greenhouse, and charging stations. A Brayton cycle is employed to generate electricity and help run the TEAS and RC. TEAS is utilized to provide cooling to the residential buildings and cold store, and hot water to the residential buildings. An ORC uses the two sources to provide electricity. Any excess electricity can be used in the electrolyzer system to produce hydrogen to be supplied to the refueling stations. The molten salt, 60% $NaNO_3$ 40% KNO_3 is used as a working fluid of the heliostat field solar collectors. The low temperature molten salt enters the receiver at point 6 and hot molten salt exits at point 1. The molten salt can either directly drive the ORC and SRC or be stored in the TES when demand is low or when the heat received by the receiver exceeds the demand.

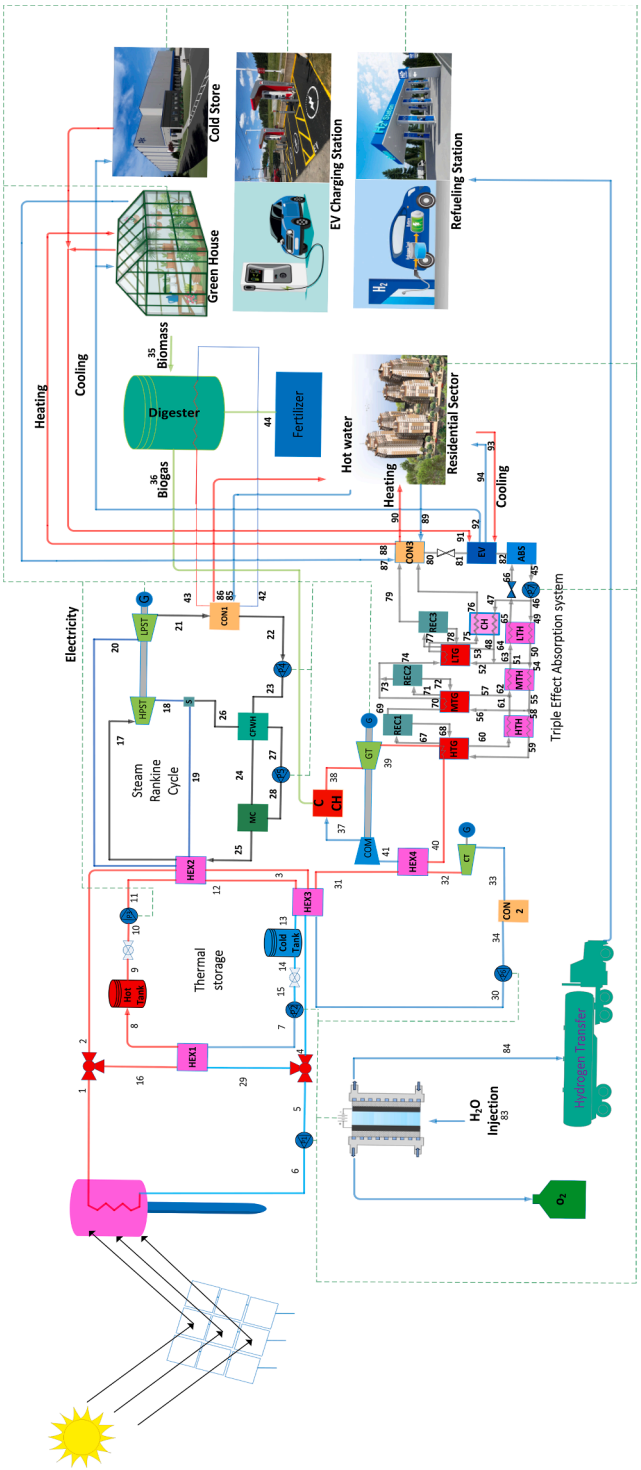

Fig. 1. Schematic of the developed multigeneration system.

The molten salt used in the solar heliostat system is also used as the substance in the TES. The TES proves beneficial when the heat demand exceeds the heat received by the receiver in the solar heliostat system or during periods without sunlight, such as at night or during snowy weather. In the SRC, the superheated high-pressure water (state 17) leaves the steam generator (HEX2) and flows to the high-pressure steam turbine (HPST). The superheated water turns the HPST and experiences a decrease in pressure and temperature. A portion of the steam exits at state 18 can be reheated in the steam generator to enter the low-pressure steam turbine (LPST) at state 20. It then passes through condenser 1 (CON1), pump 4 (P4), closed feedwater heater (CFWH), pump 5 (P5), and the mixing chamber (MC). The SRC condenser can generate heating and hot water and also acts as a heat exchanger to provide the required heat for the digestion unit.

The digester, commonly known in landfill technology, is a widely used waste treatment process that produces methane, a key component of natural gas. This study focuses on utilizing an anaerobic digestion unit to produce biogas and digestate from food waste as the biomass source. However, various biomass sources can be utilized, including municipal waste, sludge, animal manure, agricultural waste, and food waste. The biomass enters the digester at state 35 (with 25 ℃) and exits as biogas and fertilizer at state 36 (with 35 ℃) and state 44 (with 35 ℃), respectively. The fertilizer can be used for agricultural purposes, and the biogas can be used in the combustion chamber of the Brayton cycle. The working fluid in the closed Brayton cycle is air. Low-temperature air enters the combustion chamber (CCH) at state 37, and high-temperature air exits at state 38.

A portion of the heat converts to electricity via the gas turbine generator. The Brayton cycle plays a crucial role in the proposed system as it generates electricity and assists in the operation of the TEAS and ORC. The working fluid in the organic Rankine cycle is isobutane. The isobutane, at state 30, passes through heat exchangers 3 and 4 before entering the turbine (CT) at state 32, where it drives the turbine generator to produce electricity. In the TEAS, the working fluid is a mixture of ammonia and water. Water acts as the absorbent, while ammonia functions as the refrigerant. At state 59, the concentrated solution is fed into the high-temperature generator (HTG) to utilize the heat produced by the Brayton cycle.

As mentioned earlier, the system proposed in this study incorporates multiple energy conversion substances, including the SRC, BC, and ORC, to generate electricity as a product for the residential community. Any excess electricity generated can be redirected to a PEM electrolyzer system for hydrogen production. The produced hydrogen can then be transported to refueling stations to be used in hydrogen-based vehicles, promoting a sustainable mode of transportation. This aspect of the system not only provides a clean energy source for the residential community but also contributes to the reduction of carbon emissions in the transportation sector.

3. Thermodynamic analysis

The analysis and assessment of the proposed system require some

assumptions made, such as:

- The system and its individual components are operating in a steady-state condition.
- The negligible kinetic energy changes and gravitational potential energy changes take place.
- The pressure losses in pipelines and heat exchangers are disregarded.
- The isentropic efficiencies of both pumps and turbines are assumed to be 0.85 [15,16].

3.1. Solar heliostat system equations

A solar heliostat is a device that concentrates sunlight onto a specific target, such as a solar receiver or central tower, typically used in solar power plants. By utilizing mirrors, heliostats reflect and focus sunlight onto a fixed point, increasing the intensity of the sunlight and enabling the capture of a greater amount of energy. This technology is commonly employed in concentrated solar power systems, where arrays of heliostats are used to concentrate sunlight onto a solar receiver. The receiver then converts the concentrated sunlight into heat or electricity. Heliostats can be designed to track the movement of the sun throughout the day, ensuring optimal reflection angles and maximizing energy output. While heliostats have been in use for many years, recent technological advancements have improved their efficiency and cost-effectiveness, leading to their increasing adoption for large-scale solar power generation.

The heat received by the solar receiver and the rate of heat received from solar irradiation in the solar heliostat system can be determined using the following equations (see details available elsewhere [17,18,19]):

$$\dot{Q}_{rec=}\eta_h\dot{Q}_s \tag{1}$$

$$\dot{Q}_{s=}IA_{field} \tag{2}$$

where η_h and I are the efficiency of the heliostat field, and solar radiation, respectively.

The heat received by receiver can be determined as:

$$\dot{Q}_{rec=}\dot{Q}_{rec,abs}+\dot{Q}_{total.\ loss} \tag{3}$$

where $\dot{Q}_{rec,abs}$ and $\dot{Q}_{total.\ loss}$ are absorbed heat rate and the total heat losses in the receiver, respectively.

The absorbed heat rate can be explained as:

$$\dot{Q}_{rec,abs}=\dot{m}_{ms}C_p(T_{ms,out}-T_{ms,\ in}) \tag{4}$$

The total heat losses in the receiver can be determined as:

$$\dot{Q}_{total.\ lost}=\dot{Q}_{rec,em}+\dot{Q}_{rec,ref}+\dot{Q}_{rec,conv}+\dot{Q}_{rec,cond} \tag{5}$$

where $\dot{Q}_{rec,em}$, $\dot{Q}_{rec,ref}$, $\dot{Q}_{rec,conv}$ and $\dot{Q}_{rec,cond}$ are heat losses due to emissivity, reflection, convection and conduction, respectively. These losses can be determined as follows:

$$\dot{Q}_{rec,em}=\frac{\varepsilon_{avg}\sigma(T_{rec,surf}{}^4-T_0{}^4)A_{field}}{C} \tag{6}$$

$$\dot{Q}_{rec,ref}=\frac{\dot{Q}_{rec}\rho F_r}{A_{field}} \tag{7}$$

$$\dot{Q}_{rec,conv}=\frac{(h_{air,fc,insu}(T_{rec,surf}-T_0)+h_{air,nc,insu}(T_{rec,surf}-T_0))A_{field}}{CF_r} \tag{8}$$

$$\dot{Q}_{rec,cond}=\frac{(T_{rec,surf}-T_0)A_{field}}{(\frac{\delta_{insu}}{\lambda_{insu}}+\frac{1}{h_{air,o}})CF_r} \tag{9}$$

where ε_{avg}, C and F_r are average emissivity of the receiver, concentration ratio, and view factor, respectively.

$$\varepsilon_{avg}=\frac{\varepsilon_w}{\varepsilon_w+(1-\varepsilon_w)F_r} \tag{10}$$

$$C=\frac{A_{field}}{A_{ape}} \tag{11}$$

$$F_r=\frac{A_{ape}}{A_{rec,surf}} \tag{12}$$

The energetic and exergetic efficiencies of the receiver and heliostat field may be calculated as below:

$$\eta_{rec}=\frac{\dot{Q}_{rec,abs}}{\dot{Q}_{rec}} \tag{13}$$

$$\psi_{rec}=\frac{\dot{E}x_{rec,abs}}{\dot{E}x_{rec}} \tag{14}$$

$$\eta_h=\frac{\dot{Q}_{rec,abs}}{\dot{Q}_s} \tag{15}$$

$$\psi_h=\frac{\dot{E}x_{rec,abs}}{\dot{E}x_s} \tag{16}$$

3.2. Thermal energy storage system balance equations

The thermal energy storage system (TES) is designed to store the excess heat generated by the solar section [20]. This stored heat can be utilized during nighttime or when the heat demand exceeds the capacity of the energy sources [21]. However, in this study, it is assumed that during the daytime, the energy sources are capable of meeting the demands without relying on the TES. Therefore, the TES is specifically intended to function during periods when sunlight is insufficient, such as at nighttime or during rainy weather, ensuring that there is a backup source of heat available when needed. The mass, energy, exergy, and entropy balance equations for the components may be explained as follows:

For HEX1:

$$\dot{m}_8=\dot{m}_7 \tag{17}$$

$$\dot{m}_7h_7+\dot{Q}_{HEX1}=\dot{m}_8h_8 \text{ or } \dot{m}_{16}h_{16}=\dot{m}_{29}h_{29}+\dot{Q}_{HEX1} \tag{18}$$

$$\dot{m}_7ex_7+\dot{m}_{16}ex_{16}=\dot{m}_8ex_8+\dot{m}_{29}ex_{29}+\dot{E}xd_{HEX1} \tag{19}$$

$$\dot{m}_7s_7+\dot{m}_{16}s_{16}+\dot{S}_{g,HEX1}=\dot{m}_8s_8+\dot{m}_{29}s_{29} \tag{20}$$

For HEX 3:

$$\dot{m}_{12}=\dot{m}_{13} \tag{21}$$

$$\dot{m}_{12}h_{12}+\dot{m}_3h_3=\dot{m}_{13}h_{13}+\dot{m}_{14}h_{14}+\dot{Q}_{HEX3} \tag{22}$$

$$\dot{m}_{12}ex_{12}+\dot{m}_3ex_3+\dot{m}_{30}ex_{30}=\dot{m}_{13}ex_{13}+\dot{m}_4ex_4+\dot{m}_{31}ex_{31}+\dot{E}xd_{HEX3} \tag{23}$$

$$\dot{m}_{12}s_{12}+\dot{m}_3s_3+\dot{S}_{g,HEX3}=\dot{m}_{13}s_{13}+\dot{m}_4s_4+\frac{\dot{Q}_{HEX3}}{T_{HEX3}} \tag{24}$$

For Pump 2:

$$\dot{m}_{15}=\dot{m}_7 \tag{25}$$

$$\dot{m}_{15}h_{15}+\dot{W}_{P2}=\dot{m}_7h_7 \tag{26}$$

$$\dot{m}_{15}ex_{15}+\dot{W}_{P2}=\dot{m}_7ex_7+\dot{E}xd_{P2} \tag{27}$$

$$\dot{m}_{15}s_{15} + \dot{S}_{g,P2} = \dot{m}_7 s_7 \quad (28)$$

For Pump 3:

$$\dot{m}_{10} = \dot{m}_{11} \quad (29)$$

$$\dot{m}_{10}h_{10} + \dot{W}_{P3} = \dot{m}_{11}h_{11} \quad (30)$$

$$\dot{m}_{10}ex_{10} + \dot{W}_{P3} = \dot{m}_{11}ex_{11} + \dot{E}xd_{P3} \quad (31)$$

$$\dot{m}_{10}s_{10} + \dot{S}_{g,P3} = \dot{m}_{11}s_{11} \quad (32)$$

3.3. Digester balance equations

For this study, an anaerobic digestion unit was chosen. Anaerobic digestion units employ microorganisms to break down organic matter in the absence of oxygen, resulting in the production of biogas, which serves as a renewable energy source [22]. These units are capable of processing various types of organic waste materials, including sludge, agricultural waste, and food waste, offering an environmentally sustainable approach to waste management [23]. The biogas generated through anaerobic digestion can be harnessed for heat generation, electricity production, or as a transportation fuel. As such, anaerobic digestion units hold promise as a solution to meet our energy needs while simultaneously reducing waste generation and greenhouse gas emissions. In this study, particular emphasis is placed on the utilization of food waste as a biomass source for anaerobic digestion. The thermodynamics balance equations for the digestion unit are given below:

$$\dot{m}_{35,dm} = \dot{m}_{36} + \dot{m}_{44,dm} \quad (33)$$

$$ex = ex^{ch} + ex^{ph} \quad (34)$$

where ex^{ch} and ex^{ph} represent chemical and physical exergies of organic streams, respectively. The specific chemical exergies of organic streams can be determined as [24]:

$$ex^{ch} = 362.0083C + 1101.841H - 86.218O + 2.418N + 196.701S - 21.1A \quad (35)$$

where C, H, O, N, S and A stands for percentage of carbon, hydrogen, oxygen, nitrogen, sulfur and ash, respectively. These are elements of the biomass and digestate as shown in Table 1.

The specific physical exergies of organic streams can be found as below:

$$ex^{ph} = C_p\left(T - T_0 - T_0\ln\left(\frac{T}{T_0}\right)\right) \quad (36)$$

The chemical and physical exergies of the gas streams can be found below:

$$ex^{ch} = n\left(\sum_i y_i \varepsilon_i + RT_0\sum_i y_i \ln(y_i)\right) \quad (37)$$

$$ex^{ph} = C_p\left(T - T_0 - T_0\ln\left(\frac{T}{T_0}\right)\right) + RT_0\ln\left(\frac{P}{P_0}\right) \quad (38)$$

Table 1
Chemical composition of raw biomass and digestate considering moisture free analysis (data complied from [8]).

Element (%W dm)	Raw Biomass	Digestate
C	46.1	42.1
H	5.7	5.2
O	0.17	5.81
N	40.76	20.38
S	1.74	0.91
A	5.5	25.6

The exergy destruction of the digester can be calculated as follows:

$$\dot{m}_{35}ex^{ch}_{35,dm} + \dot{Q}_{HEX,\,Dig}\left(1 - \frac{T_0}{T_{Dig}}\right) = \dot{m}_{36}ex^{ch}_{36} + \dot{m}_{44,dm}ex^{ch}_{44,dm} + \dot{E}xd_{Dig} \quad (39)$$

where $\dot{Q}_{HEX,\,Dig}$ can be found as follows:

$$\dot{Q}_{HEX,\,Dig} = \dot{m}_{35}C_p(T_{Dig} - T_0) \quad (40)$$

The necessary heat for the system can be supplied by the condenser of the steam Rankine cycle. Table 1 provides information on the chemical composition of digestate and biomass. For detailed information regarding the chemical composition and the calculation methods for chemical exergy, one may refer to sources [25] and [26].

The energetic and exergetic efficiencies of the digester can be determined as follows:

$$\eta_{Dig} = \frac{\dot{m}_{36\times LHV_{Biogas}} + \dot{m}_{44,dm}LHV_{Digestate}}{\dot{m}_{35,dm}LHV_{Biomass} + \dot{Q}_{HEX,\,Dig}} \quad (41)$$

and

$$\Psi_{Dig} = \frac{\dot{m}_{36}ex^{ch}_{36} + \dot{m}_{44,dm}ex^{ch}_{44,dm}}{\dot{m}_{35}ex^{ch}_{35,dm} + \dot{Q}_{HEX,\,Dig}\left(1 - \frac{T_0}{T_{Dig}}\right)} \quad (42)$$

3.4. Brayton cycle balance equations

The Brayton cycle gains heat from the digester unit to produce electricity. Additionally, the Brayton cycle transfers heat to the organic Rankine cycle (ORC) and the triple effect absorption system (TEAS). The substance in this closed cycle is air. The main components of the Brayton cycle are the combustion chamber (CCH), gas turbine (GT), heat exchanger (HEX4), and compressor (COM). The balance equations for the main components of the Brayton cycle are presented below.

For CCH:

$$\dot{m}_{37} = \dot{m}_{38} \quad (43)$$

$$\dot{m}_{37}h_{37} + \dot{Q}_{CCH} = \dot{m}_{38}h_{38} \quad (44)$$

where $\dot{Q}_{CCH}$ is the heat provided by the biogas exited from digestion unit and can be determined as:

$$\dot{Q}_{CCH} = \dot{m}_{36,CH_4}LHV_{CH_4}\eta_{CCH} \quad (45)$$

where LHV_{CH_4} and η_{CCH} are lower heating value of the CH_4 and efficiency of the combustion chamber, respectively.

$$\dot{m}_{37}s_{37} + \frac{\dot{Q}_{CCH}}{T_{CCH}} + \dot{S}_{g,CCH} = \dot{m}_{38}s_{38} \quad (46)$$

$$\dot{m}_{37}ex_{37} + \dot{m}_{CH_4}ex^{ch}_{CH_4} + \dot{m}_{36}ex_{36} + \dot{m}_{O_2}ex^{ch}_{O_2} = \dot{m}_{38}ex_{38} + \dot{m}_{H_2O}ex^{ch}_{H_2O} + \dot{m}_{CO_2}ex^{ch}_{CO_2} + \dot{E}xd_{CCH} \quad (47)$$

where $ex^{ch}_{CH_4}$, $ex^{ch}_{O_2}$, $ex^{ch}_{H_2O}$ and $ex^{ch}_{CO_2}$ are specific chemical exergies of the CH_4 , O_2 , H_2O and CO_2 , respectively. These specific chemical exergies are tabulated in Table 2.

For GS:

$$\dot{m}_{38} = \dot{m}_{39} \quad (48)$$

Table 2
Specific chemical exergies of chemical compounds.

Compounds	Specific chemical exergy (kJ/kg)
CH_4	51,950
O_2	124.06
H_2O	527.78
CO_2	442.73

$$\dot{m}_{38}h_{38} = \dot{m}_{39}h_{39} + \dot{W}_{GT} \quad (49)$$

$$\dot{m}_{38}ex_{38} = \dot{m}_{39}ex_{39} + \dot{W}_{GT} + \dot{E}xd_{GT} \quad (50)$$

$$\dot{m}_{38}s_{38} + \dot{S}_{g,GT} = \dot{m}_{39}s_{39} \quad (51)$$

For COM:

$$\dot{m}_{41} = \dot{m}_{37} \quad (52)$$

$$\dot{m}_{41}h_{41} + \dot{W}_{COM} = \dot{m}_{37}h_{37} \quad (53)$$

$$\dot{m}_{41}ex_{41} + \dot{W}_{COM} = \dot{m}_{37}ex_{37} + \dot{E}xd_{COM} \quad (54)$$

$$\dot{m}_{41}s_{41} + \dot{S}_{g,COM} = \dot{m}_{37}s_{37} \quad (55)$$

3.5. Steam Rankine cycle balance equations

The steam Rankine cycle (SRC) utilizes the heat obtained from the heliostat field to produce electricity and heating. The working substance in this cycle is steam. The SRC consists of several key components, including a high-pressure steam turbine (HPST), a low-pressure steam turbine (LPST), a condenser (CON), a closed feedwater heater (CFWH), a mixing chamber (MC), a pump (P), and a steam generator or heat exchanger (HEX2). The thermodynamic equations for each of these components are described below.

For HEX2:

$\dot{m}_{17} = \dot{m}_{25}$ and $\dot{m}_{20} = \dot{m}_{19}$ (56).

$$\dot{m}_{25}h_{25} + \dot{m}_{19}h_{19} + \dot{Q}_{HEX2} = \dot{m}_{17}h_{17} + \dot{m}_{20}h_{20} \quad (57)$$

$$\dot{m}_{25}h_{25} + \dot{m}_{19}h_{19} + \dot{Q}_{HEX2} = \dot{m}_{17}h_{17} + \dot{m}_{20}h_{20} \quad (58)$$

$$\dot{m}_{25}s_{25} + \dot{m}_{19}s_{19} + \frac{\dot{Q}_{HEX2}}{T_{HEX2}} + \dot{S}_{g,HEX2} = \dot{m}_{17}s_{17} + \dot{m}_{20}s_{20} \quad (59)$$

For HPST:

$$\dot{m}_{17} = \dot{m}_{18} \quad (60)$$

$$\dot{m}_{17}h_{17} = \dot{m}_{18}h_{18} + \dot{W}_{HPST} \quad (61)$$

$$\dot{m}_{17}ex_{17} = \dot{m}_{18}ex_{18} + \dot{W}_{HPST} + \dot{E}xd_{HPST} \quad (62)$$

$$\dot{m}_{17}s_{17} + \dot{S}_{g,HPST} = \dot{m}_{18}s_{18} \quad (63)$$

For LPST.

$$\dot{m}_{20} = \dot{m}_{21} \quad (64)$$

$$\dot{m}_{20}h_{20} = \dot{m}_{21}h_{21} + \dot{W}_{LPST} \quad (65)$$

$$\dot{m}_{20}ex_{20} = \dot{m}_{21}ex_{21} + \dot{W}_{LPST} + \dot{E}xd_{LPST} \quad (66)$$

$$\dot{m}_{20}s_{20} + \dot{S}_{g,LPST} = \dot{m}_{21}s_{21} \quad (67)$$

For CON1:

$$\dot{m}_{22} = \dot{m}_{21} \quad (68)$$

$$\dot{m}_{21}h_{21} = \dot{m}_{22}h_{22} + \dot{Q}_{CON1} \quad (69)$$

$$\dot{m}_{21}ex_{21} + \dot{m}_{42}ex_{42} + \dot{m}_{85}ex_{85} = \dot{m}_{22}ex_{22} + \dot{m}_{43}ex_{43} + \dot{m}_{86}ex_{86} + \dot{E}xd_{CON1} \quad (70)$$

$$\dot{m}_{21}s_{21} + \dot{S}_{g,CON1} = \dot{m}_{22}s_{22} + \frac{\dot{Q}_{CON1}}{T_{CON1}} \quad (71)$$

For CFWH:

$\dot{m}_{26} = \dot{m}_{27}$ and $\dot{m}_{23} = \dot{m}_{24}$ (72).

$$\dot{m}_{23}h_{23} + \dot{Q}_{CFWH} = \dot{m}_{24}h_{24} \quad (73)$$

$$\dot{m}_{26}ex_{26} + \dot{m}_{23}ex_{23} = \dot{m}_{27}ex_{27} + \dot{m}_{24}ex_{24} + \dot{E}xd_{CFWH} \quad (74)$$

$$\dot{m}_{26}s_{26} + \dot{m}_{23}s_{23} + \dot{S}_{g,CFWH} = \dot{m}_{27}s_{27} + \dot{m}_{24}s_{24} \quad (75)$$

For pump 4:

$$\dot{m}_{22} = \dot{m}_{23} \quad (76)$$

$$\dot{m}_{22}h_{22} + \dot{W}_{P4} = \dot{m}_{23}h_{23} \quad (77)$$

$$\dot{m}_{22}ex_{22} + \dot{W}_{P4} = \dot{m}_{23}ex_{23} + \dot{E}xd_{P4} \quad (78)$$

$$\dot{m}_{22}s_{22} + \dot{S}_{g,P4} = \dot{m}_{23}s_{23} \quad (79)$$

For pump 5:

$$\dot{m}_{27} = \dot{m}_{28} \quad (80)$$

$$\dot{m}_{27}h_{27} + \dot{W}_{P5} = \dot{m}_{28}h_{28} \quad (81)$$

$$\dot{m}_{27}ex_{27} + \dot{W}_{P5} = \dot{m}_{28}ex_{28} + \dot{E}xd_{P5} \quad (82)$$

$$\dot{m}_{27}s_{27} + \dot{S}_{g,P5} = \dot{m}_{28}s_{28} \quad (83)$$

For mixing chamber (MC):

$$\dot{m}_{25} = \dot{m}_{24} + \dot{m}_{28} \quad (84)$$

$$\dot{m}_{28}h_{28} + \dot{m}_{24}h_{24} = \dot{m}_{25}h_{25} \quad (85)$$

$$\dot{m}_{28}ex_{28} + \dot{m}_{24}ex_{24} = \dot{m}_{25}ex_{25} + \dot{E}xd_{MC} \quad (86)$$

$$\dot{m}_{28}s_{28} + \dot{m}_{24}s_{24} + \dot{S}_{g,MC} = \dot{m}_{25}s_{25} \quad (87)$$

3.6. Organic Rankine cycle balance equations

The ORC utilizes the heat from the heliostat field and the digester to generate electricity and heating. Isobutane serves as the working fluid in this cycle, and the main components include a turbine, a condenser, a pump, and two heat exchangers. The mass, energy, exergy, and entropy balance equations for these components can be explained as follows:

For HEX4:

$$\dot{m}_{31} = \dot{m}_{32} \quad (88)$$

$$\dot{m}_{31}h_{31} + \dot{Q}_{HEX4} = \dot{m}_{32}h_{32} \quad (89)$$

$$\dot{m}_{31}ex_{31} + \dot{m}_{40}ex_{40} = \dot{m}_{32}ex_{32} + \dot{m}_{41}ex_{41} + \dot{E}xd_{HEX4} \quad (90)$$

$$\dot{m}_{31}s_{31} + \dot{m}_{40}s_{40} + \dot{S}_{g,HEX4} = \dot{m}_{32}s_{32} + \dot{m}_{41}s_{41} \quad (91)$$

For ORC Turbine:

$$\dot{m}_{32} = \dot{m}_{33} \quad (92)$$

$$\dot{m}_{32}h_{32} = \dot{m}_{33}h_{33} + \dot{W}_{CT} \quad (93)$$

$$\dot{m}_{32}ex_{32} = \dot{m}_{33}ex_{33} + \dot{W}_{CT} + \dot{E}xd_{CT} \quad (94)$$

$$\dot{m}_{32}s_{32} + \dot{S}_{g,CT} = \dot{m}_{33}s_{33} \quad (95)$$

For CON2:

$$\dot{m}_{33} = \dot{m}_{34} \quad (96)$$

$$\dot{m}_{33}h_{33} = \dot{m}_{34}h_{34} + \dot{Q}_{CON2} \quad (97)$$

$$\dot{m}_{33}ex_{33} = \dot{m}_{34}ex_{34} + \dot{E}xd_{CON2} \quad (98)$$

$$\dot{m}_{33}s_{33} + \dot{S}_{g,CON2} = \dot{m}_{34}s_{34} + \frac{\dot{Q}_{CON2}}{T_{CON2}} \quad (99)$$

For pump 6:

$$\dot{m}_{34} = \dot{m}_{30} \quad (100)$$

$$\dot{m}_{34}h_{34} + \dot{W}_{P6} = \dot{m}_{30}h_{30} \quad (101)$$

$$\dot{m}_{34}ex_{34} + \dot{W}_{P6} = \dot{m}_{30}ex_{30} + \dot{E}xd_{P6} \quad (102)$$

$$\dot{m}_{34}s_{34} + \dot{S}_{g,P6} = \dot{m}_{30}s_{30} \quad (103)$$

3.7. Triple effect absorption system balance equations

The main purpose of employing the triple effect absorption system (TEAS) is to provide cooling for the residential sector, greenhouse, and cold storage. Furthermore, the system can provide hot water for residential use. The working fluid in the TEAS is a mixture of ammonia and water. The mass, energy, exergy, and entropy balance equations for components may be explained as below [27]:

For HTG:

$$\dot{m}_{59+}\dot{m}_{68} = \dot{m}_{60} + \dot{m}_{67} \quad (104)$$

$$\dot{m}_{59}h_{59} + \dot{m}_{68}h_{68} + \dot{Q}_{HTG} = \dot{m}_{60}h_{60} + \dot{m}_{67}h_{67} \quad (105)$$

$$\dot{m}_{59}ex_{59} + \dot{m}_{68}ex_{68} + \dot{m}_{39}ex_{39} = \dot{m}_{60}ex_{60} + \dot{m}_{67}ex_{67} + \dot{m}_{40}ex_{40} + \dot{E}xd_{HTG} \quad (106)$$

$$\dot{m}_{59}s_{59} + \dot{m}_{68}s_{68} + \frac{\dot{Q}_{HTG}}{T_{HTG}} + \dot{S}_{g,HTG} = \dot{m}_{60}s_{60} + \dot{m}_{67}s_{67} \quad (107)$$

For MTG:

$$\dot{m}_{56} + \dot{m}_{72} = \dot{m}_{57} + \dot{m}_{71} \quad (108)$$

$$\dot{m}_{56}h_{56} + \dot{m}_{72}h_{72} + \dot{Q}_{MTG} = \dot{m}_{57}h_{57} + \dot{m}_{71}h_{71} \quad (109)$$

$$\dot{m}_{56}ex_{56} + \dot{m}_{72}ex_{72} + \dot{m}_{69}ex_{69} = \dot{m}_{57}ex_{57} + \dot{m}_{71}ex_{71} + \dot{m}_{70}ex_{70} + \dot{E}xd_{MTG} \quad (110)$$

$$\dot{m}_{56}s_{56} + \dot{m}_{72}s_{72} + \frac{\dot{Q}_{MTG}}{T_{MTG}} + \dot{S}_{g,MTG} = \dot{m}_{57}s_{57} + \dot{m}_{71}s_{71} \quad (111)$$

For LTG:

$$\dot{m}_{52+}\dot{m}_{77} = \dot{m}_{53} + \dot{m}_{78} \quad (112)$$

$$\dot{m}_{52}h_{52} + \dot{m}_{78}h_{78} + \dot{Q}_{LTG} = \dot{m}_{53}h_{53} + \dot{m}_{77}h_{77} \quad (113)$$

$$\dot{m}_{52}ex_{52} + \dot{m}_{78}ex_{78} + \dot{m}_{74}ex_{74} = \dot{m}_{53}ex_{53} + \dot{m}_{77}ex_{77} + \dot{m}_{75}ex_{75} + \dot{E}xd_{LTG} \quad (114)$$

$$\dot{m}_{52}s_{52} + \dot{m}_{78}s_{78} + \frac{\dot{Q}_{LTG}}{T_{LTG}} + \dot{S}_{g,LTG} = \dot{m}_{53}s_{53} + \dot{m}_{77}s_{77} \quad (115)$$

For HTH:

$$\dot{m}_{58} = \dot{m}_{59}\text{and}\dot{m}_{60} = \dot{m}_{61}$$

$$\dot{m}_{58}h_{58} + \dot{Q}_{HTH} = \dot{m}_{59}h_{59} \quad (117)$$

$$\dot{m}_{58}ex_{58} + \dot{m}_{60}ex_{60} = \dot{m}_{59}ex_{59} + \dot{m}_{61}ex_{61} + \dot{E}xd_{HTH} \quad (118)$$

$$\dot{m}_{58}s_{58} + \frac{\dot{Q}_{HTH}}{T_{HTH}} + \dot{S}_{g,HTH} = \dot{m}_{59}s_{59} \quad (119)$$

For MTH:

$$\dot{m}_{54} = \dot{m}_{55}\text{and}\dot{m}_{62} = \dot{m}_{63}$$

$$\dot{m}_{54}h_{54} + \dot{Q}_{MTH} = \dot{m}_{55}h_{55} \quad (121)$$

$$\dot{m}_{54}ex_{54} + \dot{m}_{62}ex_{62} = \dot{m}_{55}ex_{55} + \dot{m}_{63}ex_{63} + \dot{E}xd_{MTH} \quad (122)$$

$$\dot{m}_{54}s_{54} + \frac{\dot{Q}_{MTH}}{T_{MTH}} + \dot{S}_{g,MTH} = \dot{m}_{55}s_{55} \quad (123)$$

For LTH:

$$\dot{m}_{49} = \dot{m}_{50}\text{and}\,\dot{m}_{64} = \dot{m}_{65}$$

$$\dot{m}_{49}h_{49} + \dot{Q}_{LTH} = \dot{m}_{50}h_{50} \quad (125)$$

$$\dot{m}_{49}ex_{49} + \dot{m}_{64}ex_{64} = \dot{m}_{50}ex_{50} + \dot{m}_{65}ex_{65} + \dot{E}xd_{LTH} \quad (126)$$

$$\dot{m}_{49}s_{49} + \frac{\dot{Q}_{LTH}}{T_{LTH}} + \dot{S}_{g,LTH} = \dot{m}_{50}s_{50} \quad (127)$$

For CH:

$$\dot{m}_{47} = \dot{m}_{48}\text{and}\,\dot{m}_{75} = \dot{m}_{76}$$

$$\dot{m}_{47}h_{47} + \dot{Q}_{CH} = \dot{m}_{48}h_{48} \quad (129)$$

$$\dot{m}_{47}ex_{47} + \dot{m}_{75}ex_{75} = \dot{m}_{48}ex_{48} + \dot{m}_{76}ex_{76} + \dot{E}xd_{CH} \quad (130)$$

$$\dot{m}_{47}s_{47} + \frac{\dot{Q}_{CH}}{T_{CH}} + \dot{S}_{g,CH} = \dot{m}_{48}s_{48} \quad (131)$$

For CON3:

$$\dot{m}_{80} = \dot{m}_{79} + \dot{m}_{76} \quad (132)$$

$$\dot{m}_{79}h_{79} + \dot{m}_{76}h_{76} = \dot{m}_{80}h_{80} + \dot{Q}_{CON3} \quad (133)$$

$$\dot{m}_{79}ex_{79} + \dot{m}_{76}ex_{76} + \dot{m}_{87}ex_{87} + \dot{m}_{89}ex_{89} = \dot{m}_{80}ex_{80} + \dot{m}_{88}ex_{88} + \dot{m}_{90}ex_{90} + \dot{E}xd_{CON3} \quad (134)$$

$$\dot{m}_{79}s_{79} + \dot{m}_{76}h_{76} + \dot{S}_{g,CON3} = \dot{m}_{80}s_{80} + \frac{\dot{Q}_{CON3}}{T_{CON3}} \quad (135)$$

For pump 7:

$$\dot{m}_{45} = \dot{m}_{46} \quad (136)$$

$$\dot{m}_{45}h_{45} + \dot{W}_{P7} = \dot{m}_{46}h_{46} \quad (137)$$

$$\dot{m}_{45}ex_{45} + \dot{W}_{P7} = \dot{m}_{46}ex_{46} + \dot{E}xd_{P7} \quad (138)$$

$$\dot{m}_{45}s_{45} + \dot{S}_{g,P7} = \dot{m}_{46}s_{46} \quad (139)$$

For EV:

$$\dot{m}_{81} = \dot{m}_{82} \quad (140)$$

$$\dot{m}_{81}h_{81} + \dot{Q}_{EV} = \dot{m}_{82}h_{82} \quad (141)$$

$$\dot{m}_{81}ex_{81} + \dot{m}_{91}ex_{91} + \dot{m}_{93}ex_{93} = \dot{m}_{82}ex_{82} + \dot{m}_{92}ex_{92} + \dot{m}_{94}ex_{94} + \dot{E}xd_{EV} \quad (142)$$

$$\dot{m}_{81}s_{81} + \frac{\dot{Q}_{EV}}{T_{EV}} + \dot{S}_{g,EV} = \dot{m}_{82}s_{82} \quad (143)$$

For ABS:

$$\dot{m}_{45} = \dot{m}_{66} + \dot{m}_{82} \quad (144)$$

$$\dot{m}_{66}h_{66} + \dot{m}_{82}h_{82} = \dot{m}_{45}h_{45} + \dot{Q}_{ABS} \quad (145)$$

$$\dot{m}_{66}ex_{66} + \dot{m}_{82}ex_{82} = \dot{m}_{45}ex_{45} + \dot{E}xd_{ABS} \quad (146)$$

$$\dot{m}_{66}s_{66} + \dot{m}_{82}h_{82} + \dot{S}_{g,ABS} = \dot{m}_{45}s_{45} + \frac{\dot{Q}_{ABS}}{T_{ABS}} \quad (147)$$

3.8. PEM electrolyzer equations

A PEM (proton exchange membrane) type electrolyzer is considered in the current system. The PEM is an electrolysis system that employs a solid polymer electrolyte membrane to generate hydrogen from water. This technology uses an electrical current to separate water molecules into oxygen and hydrogen, which can then be used as a source of clean energy [28]. The PEM electrolyzer is an attractive option for hydrogen production due to its high efficiency and low operating temperatures [29]. Unlike other types of electrolysis systems, PEM electrolyzer does not require high pressure or temperatures, making them safer and easier to operate. Additionally, the PEM electrolyzer is highly versatile and can be used in a variety of applications, from small-scale energy production to large industrial applications. The generated hydrogen in the PEM can be calculated as follows:

$$\frac{.\mathbf{m}_{H_2} = \eta_{Elec}{}^{*}.\mathbf{W}_{Elec}}{\mathbf{HHV}_{hyd}} \quad (148)$$

where η_{Elec} and HHV_{hyd} refer hydrogen production efficiency and higher heating value of hydrogen, respectively.

The produced hydrogen has exergy flow rate as expressed below:

$$\dot{\mathbf{ex}}_{H_2} = \dot{\mathbf{m}}_{H_2}[\mathbf{ex}_{H_2,ch} + \mathbf{ex}_{H_2,ph}] \quad (149)$$

where $ex_{H_2,ph}$ and $ex_{H_2,ch}$ represent physical and chemical exergy of hydrogen respectively. The equations are provided as follows:

$$\mathbf{ex}_{H_2,ph} = (\mathbf{h}_{H_2} - \mathbf{h}_0) - \mathbf{t}_0(\mathbf{s}_{H_2} - \mathbf{s}_0) \quad (150)$$

and

$$\mathbf{ex}_{H_2,ch} = \frac{236100}{\mathbf{MW}_{H_2}} \quad (151)$$

4. Results and discussion

Using the thermodynamic analysis methodology by writing all balance equations of mass, energy, entropy and exergy for the system itself and its components accordingly, we have been able to make the necessary design calculations and develop the system in a conceptually correct manner where the thermodynamic concepts and the thermodynamic laws are fully satisfied. In this regard, Table 3 tabulates all obtained properties for the state points in the presently developed system, which are utilized to assess the system's output and conduct parametric studies.

4.1. Effect of molar fraction of CH_4 in biogas on different parameters

The biogas studied in this analysis contains both CO_2 and CH_4. The molar fraction of CH_4, which is inversely related to the fraction of CO_2, affects both specific chemical exergy and the heating value of the biogas. These factors, in turn, impact the energetic and exergetic performance of biogas-fueled Brayton power generation.

In Fig. 2, it is shown how the molar fraction of methane affects the lower heating value and specific chemical exergy of biogas. The lower heating value of biogas increases from 20,009 kJ/kg to 40,018 kJ/kg as the molar fraction of methane increases from 0.4 to 0.8. Additionally, the specific chemical exergy of biogas increases from 538.6 kJ/kg to 3219 kJ/kg with the same increase in methane molar fraction.

Fig. 3 illustrates the effects of biogas quality on the energy and exergy efficiencies of the Brayton cycle and digester unit. As shown, by increasing the molar fraction of CH_4 in biogas from 0.4 to 0.8, the energy efficiencies of the Brayton cycle and digester unit increase from 13.6% to 35.15% and from 72.11% to 83.94%, respectively.

4.2. Effect of HPST inlet temperature on the SRC efficiencies

In the context of designing and operating an SRC (referring to: solar Rankine cycle) system, the inlet temperature plays a crucial role in calculating the system efficiencies and outputs. The effect of the inlet temperature on the high-pressure steam turbine (HPST) can be found in Fig. 4. The figure shows that when the inlet temperature of the HPST is increased from 690 K to 790 K, there is an increase in both the energy and exergy efficiencies of the SRC. The energy efficiency of the SRC increases from approximately 34% to 36%, while the exergy efficiency increases from approximately 73% to 74 %, respectively. This increase in efficiency may be attributed to the fact that when the inlet temperature of the turbine is increased, the temperature difference between the hot fluid and the surroundings also increases. This temperature difference leads to a higher amount of energy being extracted from the fluid, resulting in an increase in the work output of the turbine. Moreover, the increase in work output can be utilized to generate more electricity for the same amount of fuel input. This results in a higher overall efficiency of the power generation system, as more of the fuel's energy is being converted into useful work. Therefore, increasing the inlet temperature of the turbine is an effective approach to enhancing the energetic efficiency of the SRC system and achieving higher power generation outputs.

It should be highlighted that raising the temperature at the turbine inlet imposes more stringent requirements on the turbine materials to prevent them from deteriorating under high temperatures. Consequently, the contemporary gas turbine designs utilize sophisticated cooling and material techniques to allow for elevated inlet temperatures while ensuring that the turbines remain robust and dependable.

4.3. Effect of ambient temperature on the energy and exergy efficiencies

The performance of thermodynamic systems, including the integrated systems studied, is significantly influenced by changes in ambient temperature, as these systems heavily rely on heat. Therefore, variations in ambient temperature should be considered when determining system performance. In fact, changes in ambient temperature can affect the efficiency and effectiveness of thermodynamic systems in various ways.

Fig. 5 provides insight into the effect of ambient temperature on the energetic and exergetic COP of the TEAS. This diagram shows that when the ambient temperature increases from 298 K to 318 K, there is an increase in the exergetic COP, while the energetic COP remains constant. This is because when the ambient temperature is low, there is a lower driving force for heat transfer, leading to a lower exergy efficiency. On the other hand, when the ambient temperature is high, the system's exergy efficiency increases due to a higher driving force for heat transfer taking place. It should be emphasized that the accuracy of the absorption system has been verified with reference to [30], where the energetic COP was found to be approximately 1.5.

Fig. 6 illustrates the effect of ambient temperature on the energy and exergy efficiencies of various subsystems, including the ORC, Brayton, and SRC. As mentioned, the ambient temperature is an important factor to consider when designing and operating thermodynamic systems, as changes in the ambient temperature can have a critical impact on system performance. As shown in the diagram, increasing the ambient temperature from 298 K to 318 K results in a slight increase in the exergy efficiencies of the ORC, Brayton, and SRC systems. Specifically, the exergy efficiencies of the ORC, Brayton, and SRC systems increase from approximately 23% to 25 %, from approximately 31.5% to 33%, and from approximately 74% to 80%, respectively. This increase in exergy efficiency is due to the higher driving force for heat transfer that occurs when the ambient temperature is higher. However, it is worth noting that the energy efficiencies of these systems remain constant, as thermal

Table 3
State point properties in the currently developed system.

State point	Fluid/substance	Temperature (K)	Pressure (kPa)	Mass flow rate (kg/s)	Specific enthalpy (kJ/kg)	Specific entropy (kJ/kgK)	Specific exergy (kJ/kg)
1	Molten Salt	838.20	100	5.67	463.30	0.68	1659.26
2	Molten Salt	838.20	100	3.02	463.30	0.68	1659.28
3	Molten Salt	709.40	100	3.02	265.80	0.43	1538.00
4	Molten Salt	701.30	100	3.02	253.50	0.41	1530.73
5	Molten Salt	701.30	100	5.67	253.50	0.41	1531.00
6	Molten Salt	701.40	120	5.60	253.50	0.41	1531.00
7	Molten Salt	568.90	300	1.40	53.67	0.09	1425.71
8	Molten Salt	830	300	1.40	450.90	0.67	1651.42
9	Molten Salt	820	101.3	1.40	435.30	0.65	1641.42
10	Molten Salt	820	101.3	1.40	435.30	0.65	1641.42
11	Molten Salt	820	300	1.40	435.40	0.65	1641.42
12	Molten Salt	589.80	300	1.40	85.03	0.15	1440.71
13	Molten Salt	576.50	300	1.40	65.03	0.11	1430.71
14	Molten Salt	568.90	101.3	1.40	53.55	0.09	1425.71
15	Molten Salt	568.90	101.3	1.40	53.55	0.09	1425.71
16	Molten Salt	838.20	100	2.65	463.30	0.68	3553.96
17	Water	790	10,112	0.33	3417	6.64	2835.42
18	Water	619.10	2953	0.33	3108	6.73	2499.40
19	Water	619.10	2953	0.29	3108	6.73	2499.32
20	Water	790	2953	0.29	3496	7.29	2722.03
21	Water	324.60	13.29	0.29	2520	7.82	1588.61
22	Water	314.60	13.29	0.29	173.70	0.59	1397.91
23	Water	314.80	2953	0.29	177.20	0.59	1400.94
24	Water	380.10	2953	0.29	450.70	1.38	1439.01
25	Water	393.20	10,112	0.33	511	1.51	1458.78
26	Water	619.10	2953	0.03	3108	6.73	2499.21
27	Water	499.10	2953	0.03	971.40	2.57	1605.26
28	Water	500.90	10,112	0.03	981.60	2.57	1614.47
29	Molten Salt	701.30	100	2.65	253.50	0.41	1531.32
30	Isobutane	276	1743	9.55	207.70	1.01	1304.84
31	Isobutane	278.90	1743	9.55	214.60	1.04	1304.32
32	Isobutane	425.60	1743	9.55	820.10	2.75	1400.35
33	Isobutane	379.70	331.90	9.55	746.90	2.78	1316.87
34	Isobutane	275.20	331.90	9.55	204.90	1.01	1302.43
35	Biomass	298	100	17.85			
36	Biogas	308	100	1.82			
37	Air	602.30	3785	42.57	609.80	5.37	408.40
38	Air	949.20	3785	42.57	988.70	5.86	639.60
39	Air	460	541.60	42.57	462.30	5.65	177.68
40	Air	426.60	541.60	42.57	428.30	5.57	166.50
41	Air	291.90	541.60	42.57	292.30	5.19	144.65
42	Water	298	100	4.20	104.30	0.36	1396.19
43	Water	318.60	100	4.20	190.50	0.64	1399.04
44	Digestate	308.20	100	16.03			
45	Ammonia-Water	272.20	317	3.37	−238.90	−0.19	1220.61
46	Ammonia-Water	272.30	972	3.37	−238	−0.19	1221.20
47	Ammonia-Water	272.30	972	1.40	−238	−0.19	1221.66
48	Ammonia-Water	285	972	1.40	−179.60	0.012	1217.39
49	Ammonia-Water	272.30	972	1.97	−238	−0.19	1221.37
50	Ammonia-Water	288.70	972	1.97	−162.60	0.07	1216.31
51	Ammonia-Water	288.70	972	0.24	−162.60	0.072	1216.64
52	Ammonia-Water	285.60	972	1.64	−177.10	0.02	1217.23
53	Ammonia-Water	295.60	972	1.09	−132.50	0.19	1209.47
54	Ammonia-Water	288.70	972	1.72	−162.60	0.072	1216.31
55	Ammonia-Water	327.30	972	1.72	68.95	0.81	1227.29
56	Ammonia-Water	327.30	972	0.43	68.95	0.81	1227.08
57	Ammonia-Water	332.90	972	0.31	32.81	0.72	1217.90
58	Ammonia-Water	327.30	972	1.29	68.95	0.81	1226.60

(*continued on next page*)

Table 3 (*continued*)

State point	Fluid/substance	Temperature (K)	Pressure (kPa)	Mass flow rate (kg/s)	Specific enthalpy (kJ/kg)	Specific entropy (kJ/kgK)	Specific exergy (kJ/kg)
59	Ammonia-Water	352.20	972	1.29	513.20	2.11	1281.51
60	Ammonia-Water	420.80	972	0.65	1593	4.73	1580.88
61	Ammonia-Water	387.30	972	0.65	711	2.57	1344.29
62	Ammonia-Water	373.20	972	0.97	487.80	1.99	1295.47
63	Ammonia-Water	342.30	972	0.97	75.10	0.84	1223.33
64	Ammonia-Water	317.60	972	2.06	−35.10	0.51	1212.76
65	Ammonia-Water	301.30	972	2.06	−107	0.28	1209.86
66	Ammonia-Water	301.50	317	2.06	−107	0.28	1209.38
67	Ammonia-Water	419.80	972	0.77	1691	5.45	1464.11
68	Ammonia-Water	419.80	972	0.13	1626	5.30	1445.46
69	Ammonia-Water	450	972	0.64	1679	5.40	1467.58
70	Ammonia-Water	361.10	972	0.64	1459	4.86	1409.91
71	Ammonia-Water	331.90	972	0.18	1175	4.04	1370.31
72	Ammonia-Water	331.90	972	0.07	825.20	3.02	1323.87
73	Ammonia-Water	328	972	0.11	1374	4.61	1398.29
74	Ammonia-Water	355.90	972	0.75	1446	4.82	1407.85
75	Ammonia-Water	297.10	972	0.75	233.80	0.81	1393.35
76	Ammonia-Water	297.10	972	0.75	125.80	0.44	1393.35
77	Ammonia-Water	294.60	972	0.65	−108.10	0.19	1235.98
78	Ammonia-Water	294.60	972	0.10	−130.90	0.16	1220.40
79	Ammonia-Water	340	972	0.55	1405	4.71	1401.81
80	Ammonia-Water	295	972	1.30	102.40	0.36	1392.66
81	Ammonia-Water	265.30	317	1.30	102.40	0.39	1384.26
82	Ammonia-Water	294.30	317	1.30	1329	4.98	1242.17
83	Water	291.20	101	10	75.85	0.26	1396.50
84	H_2	291.20	101	0.04			
85	Water	298	100	16.64	298.40	5.69	3.79E-05
86	Water	318	100	16.60	318.50	5.76	0.60
87	Air	294.90	100	2.08	295.30	5.68	0.01
88	Air	330	100	2.08	330.60	5.80	1.56
89	Air	283.70	100	21.57	284.10	5.65	0.36
90	Air	314.20	100	21.57	314.70	5.75	0.39
91	Air	294.30	100	9.80	294.70	5.68	0.02
92	Air	278	100	9.80	278.40	5.62	0.71
93	Air	294.30	100	88.26	294.70	5.68	0.02
94	Air	278	100	88.26	278.40	5.62	0.71

losses are not taken into account in this analysis. Thermal losses refer to the energy that is lost to the environment through various forms of heat transfer, such as radiation and convection. These losses can have a significant impact on the energy efficiency of thermodynamic systems, particularly in high-temperature applications.

Furthermore, it is essential to consider the impact of changes in ambient temperature when designing and operating thermodynamic systems, as they can have a significant effect on their performance. By understanding how ambient temperature affects the system, one can take steps to optimize its performance, thus ensuring maximum efficiency and effectiveness.

4.4. Entropy generation of different components

In this section, the focus is on analyzing the entropy generations within the thermodynamic system. Entropy generation is a measure of the degree of irreversibility in a thermodynamic process. Irreversibilities are processes that cannot be reversed without significant energy input or an increase in entropy. These processes can include friction, heat transfer across a finite temperature difference, and mixing of two fluids at different temperatures. As irreversibilities occur in a thermodynamic system, they lead to an increase in entropy, which is reflected in the entropy generation of the system. As illustrated in Fig. 7, the entropy

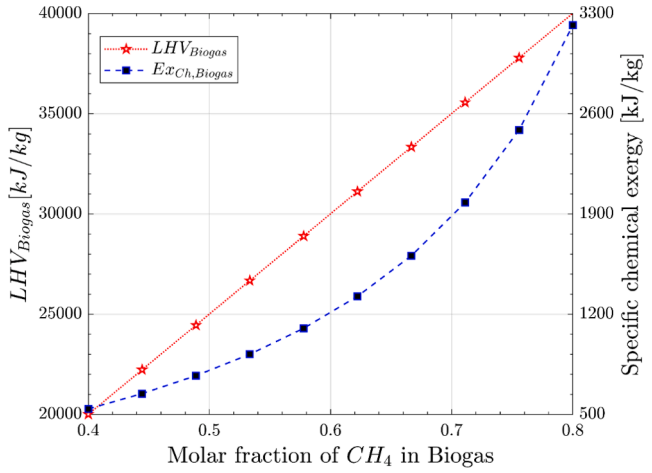

Fig. 2. Effect of biogas quality on the LHV and specific chemical exergy of Biogas.

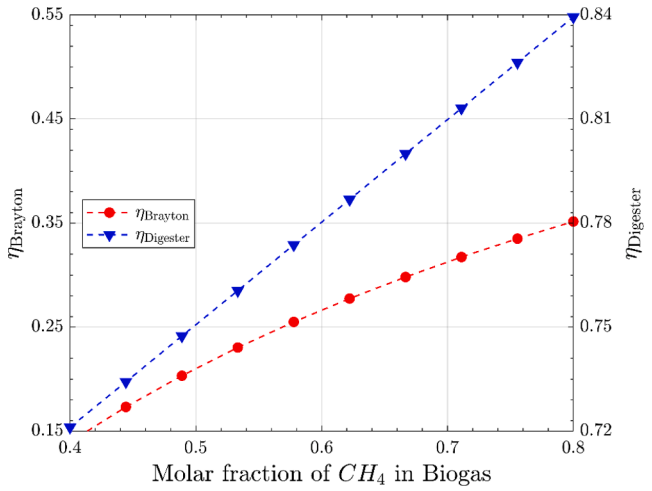

Fig. 3. Effect of biogas quality on the energy and exergy efficiencies of the Brayton cycle and digester unit.

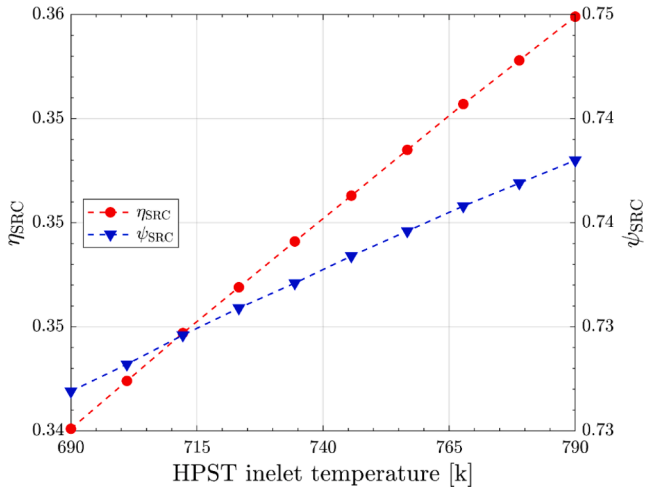

Fig. 4. Effect of HPST inlet temperature on the SRC efficiencies.

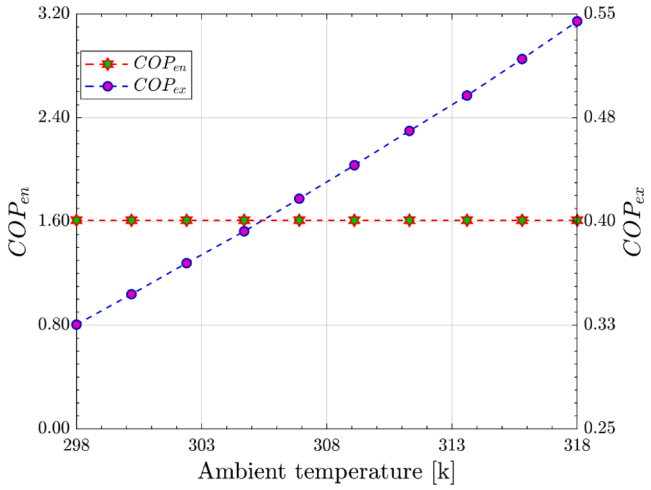

Fig. 5. Effect of ambient temperature on the energy and exergy COPs.

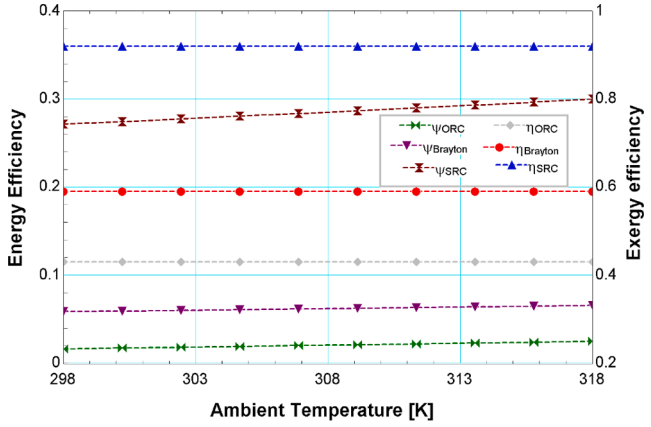

Fig. 6. Effect of ambient temperature on the energy and exergy efficiencies.

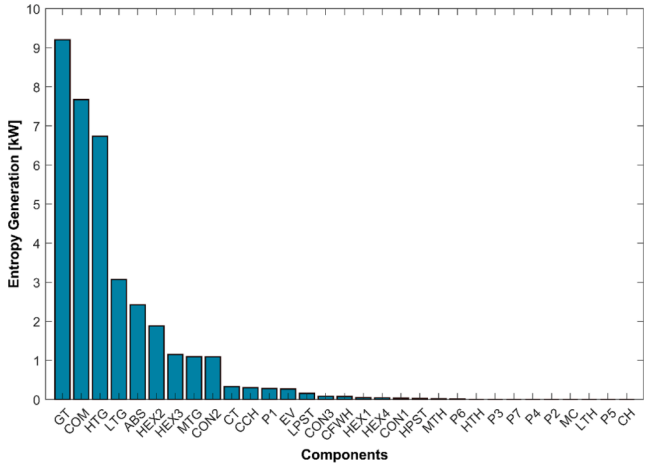

Fig. 7. Entropy generation in different components.

generations in the system are relatively low, indicating that the system is operating efficiently with minimal energy waste. The low entropy generation is a reflection of the high efficiency of the system and the effective conversion of energy to useful work. This is an important parameter in the design and operation of thermodynamic systems, as it ensures that the system is operating at its maximum potential and minimizing the amount of energy lost to the environment.

By minimizing the entropy generation within the system, the efficiency of the system can be improved, and energy waste can be reduced. This can be achieved by optimizing the design of the system, using high-quality components and materials, and minimizing the potential sources of irreversibility within the system. As such, the analysis of entropy generation is a necessary tool in the design and optimization of thermodynamic processes and can be used to identify areas of the system that may require improvement or optimization.

4.5. Exergy destruction rates

The exergy destruction rates for major components of the system have been calculated and presented in Table 4. It illustrates that the digester (Dig), compressor (COM), combustion chamber (CCH), and heat exchanger 1 (HEX1) have the highest values of exergy destruction rates due to their high temperatures and mass flow rates. The exergy destruction rates are determined for the subsystems as illustrated in Fig. 8 for digester unit (Dig), Brayton cycle (BC), thermal storage energy system (TES), Organic Rankine cycle (ORC), triple effect absorption system (TEAS), steam Rankine cycle (SRC), and electrolyzer (Elec). As shown, the exergy destruction rates for Dig, BC, TES, ORC, TEAS, SRC, and Elec are 91425, 9475.20, 2452.32, 598.48, 523.9, 113.51, and 57.04 kW, respectively.

5. Conclusions

In the current study the newly developed multigeneration system employs two different renewable energy sources, biomass and solar. The developed system utilizes food waste to produce biogas to feed the Brayton cycle. In addition, the system generates energy for multiple demands simultaneously, including heating, hot water, electricity, and cooling. Cooling can be provided for the cold storage, and heating and cooling flow to the greenhouse, depending on the season of the year. Additionally, electricity can be transferred to the charging stations to charge electric vehicles. Also, the excess electricity produced can be captured for hydrogen production to be used in the refueling stations. The multigeneration system developed in this study serves as a reference case for researchers working on the design and development of multi-generation systems. Various technical and operational aspects of the currently developed system are studied and evaluated, and some of the key results are then listed as follows:

- The energy analysis of the system is assessed, and the results show that the steam Ranking cycle, Brayton cycle, and organic Rankine cycle have energy efficiencies of 35.9%, 19.5%, and 11.49% respectively. Additionally, the absorption system has an energy COP of 1.609.
- The exergy analysis of the system reveals that the steam Ranking cycle, Brayton cycle, and organic Rankine cycle achieve exergy efficiencies of 74.3%, 31.68%, and 23.23% respectively. Furthermore, the absorption system exhibits an exergy COP of 0.3269.
- The exergy destruction rate of different components and subsystems are evaluated, and the results show that the digester, compressor, combustion chamber, and heat exchanger 1 have the highest exergy destruction rates.
- The entropy generation rates in different components are calculated, and among those, the gas turbine has the highest entropy generation rate.
- The developed system can produce hydrogen at a rate of 0.04 kg/s.

Declaration of Competing Interest

The authors declare that they have no known competing financial interests or personal relationships that could have appeared to influence the work reported in this paper.

Table 4
The exergy destruction rates calculated for different components of the current system.

Components	Exergy destruction rates (kW)	Components	Exergy destruction rates (kW)
Dig	91,425	CFWH	22.65
COM	4672	MTG	19.83
CCH	4186	LTH	14.82
HEX1	2274	HEX4	12.50
GT	617.20	P6	12.19
HEX3	337.90	HPST	8.97
EV	185.30	LTG	7.09
HTG	162.20	CH	5.79
CON2	138.10	ABS	5.37
CT	97.79	P7	4.48
HEX2	94.01	CON3	0.84
P1	83.46	P3	0.83
HTH	82.72	P4	0.14
Elec	57.04	MC	0.10
MTH	51.94	P5	0.03
LPST	46.92	P2	0.01
CON1	34.69		

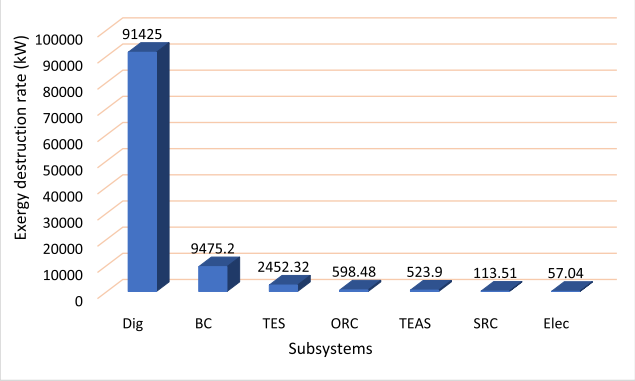

Fig. 8. Exergy destruction rates determined for the subsystems.

Data availability

The data that have been used are confidential.

References

[1] S.S. Rashwan, I. Dincer, A. Mohany, Analysis and assessment of cascaded closed loop type organic Rankine cycle, Energy Convers. Manag. 184 (2019) 416–426.
[2] M. Thirunavukkarasu, Y. Sawle, H. Lala, A comprehensive review on optimization of hybrid renewable energy systems using various optimization techniques, Renew. Sustain. Energy Rev. 176 (2023), 113192, https://doi.org/10.1016/j.rser.2023.113192.
[3] N. Ding, W. Wu, L. Wang, H. Yin, Application of nanomaterial based alkaline electrolyzer for hydrogen production in renewable energy-driven system: Multi-criteria assessment, environmental and exergoeconomic approaches, Int. J. Hydrog. Energy (2023), https://doi.org/10.1016/j.ijhydene.2023.03.364.
[4] U. Rumeysa Kelem, F. Yilmaz, Development and assessment of a novel multigeneration plant combined with a supercritical CO2 cycle for multiple products, Int. J. Hydrog. Energy (2023), https://doi.org/10.1016/j.ijhydene.2023.05.316.
[5] S.A. Klein, Engineering equation solver (EES) for microsoft windows operating system: commercial and professional versions, Madison WI F-Chart Softw. (2002).
[6] O.V. Ekechukwu, U.G. Azubuike, L.C. Egbuhuzor, H.O. Njoku, Exergy analysis of a steam power plant at full and partial load conditions, Int. J. Exergy 40 (2) (2023) 182, https://doi.org/10.1504/IJEX.2023.10053808.
[7] A. Eldeib, M. Luqman, Y. Bicer, T.A. Al-Ansari, Thermodynamic design and analysis of a multigeneration system to support sustainable dairy farming, Energy Convers. Manag. X 18 (Apr. 2023), 100363, https://doi.org/10.1016/j.ecmx.2023.100363.
[8] A.E. Karaca, I. Dincer, M. Nitefor, A unique biomass based integrated energy system for cleaner production of multiple energy outputs for sustainable communities, Sustain. Cities Soc. 89 (2023), 104330, https://doi.org/10.1016/j.scs.2022.104330.

[9] J. Zhou, M. Zoghi, H. Abed, Efficient waste heat recovery of a hybrid solar-biogas-fueled gas turbine cycle for poly-generation purpose: 4E analysis, parametric study, and multi-objective optimization, Fuel 333 (2023), 126502, https://doi.org/10.1016/j.fuel.2022.126502.
[10] O. Bamisile, D. Cai, M. Adedeji, M. Dagbasi, J. Li, Y. Hu, Q. Huang, Thermo-enviro-exergoeconomic analysis and multi-objective optimization of a novel geothermal-solar-wind micro-multi-energy system for cleaner energy production, Process Safety Environ. Protect. 170 (2023) 157–175, https://doi.org/10.1016/j.psep.2022.11.068.
[11] A. Ghasemi, P. Heidarnejad, A. Noorpoor, A novel solar-biomass based multi-generation energy system including water desalination and liquefaction of natural gas system: thermodynamic and thermoeconomic optimization, J. Clean. Prod. 196 (2018) 424–437, https://doi.org/10.1016/j.jclepro.2018.05.160.
[12] J. Wang, Z. Cui, W. Yao, S. Huo, Regulation strategies and thermodynamic analysis of combined cooling, heating, and power system integrated with biomass gasification and solid oxide fuel cell, Energy 266 (2023), 126430, https://doi.org/10.1016/j.energy.2022.126430.
[13] Z. Zhang, S.M. Alelyani, N. Zhang, C. Zeng, Y. Yuan, P.E. Phelan, Thermodynamic analysis of a novel sodium hydroxide-water solution absorption refrigeration, heating and power system for low-temperature heat sources, Appl. Energy 222 (Jul. 2018) 1–12, https://doi.org/10.1016/j.apenergy.2018.04.008.
[14] M. Sharifishourabi, E. Arab Chadegani, Performance assessment of a new organic Rankine cycle based multi-generation system integrated with a triple effect absorption system, Energy Convers. Manag. 150 (2017) 787–799, doi: 10.1016/j.enconman.2017.07.050.
[15] T.A.H. Ratlamwala, S.I. Ali, A. Riaz, S.M. Hamza, Municipal solid waste based multigeneration system for different districts of Karachi, Int. J. Exergy 29 (2–4) (2019) 300–317.
[16] D. Hjeij, Y. Biçer, M. Koç, Thermodynamic analysis of a multigeneration system using solid oxide cells for renewable power-to-X conversion, Int. J. Hydrog. Energy 48 (32) (2023) 12056–12071, https://doi.org/10.1016/j.ijhydene.2022.09.024.
[17] N. Ma, F. Meng, W. Hong, H. Li, X. Niu, Thermodynamic assessment of the dry-cooling supercritical Brayton cycle in a direct-heated solar power tower plant enabled by CO2-propane mixture, Renew. Energy 203 (2023) 649–663, https://doi.org/10.1016/j.renene.2022.12.084.
[18] Y. Liang, X. Lin, W. Su, L. Xing, N. Zhou, Thermal-economic analysis of a novel solar power tower system with CO2-based mixtures at typical days of four seasons, Energy 276 (2023), 127602, https://doi.org/10.1016/j.energy.2023.127602.
[19] E. Assareh, N. Agarwal, M.C. Paul, P. Ahmadi, M. Ghodrat, M. Lee, Investigation and development of a novel solar-biomass integrated energy system for clean electricity and liquid hydrogen production, Therm. Sci. Eng. Prog. 42 (2023), 101925, https://doi.org/10.1016/j.tsep.2023.101925.
[20] A. Tafuni, A. Giannotta, M. Mersch, A.M. Pantaleo, R. Amirante, C.N. Markides, P. De Palma, Thermo-economic analysis of a low-cost greenhouse thermal solar plant with seasonal energy storage, Energy Convers. Manage. 288 (2023), 117123, https://doi.org/10.1016/j.enconman.2023.117123.
[21] G.S. Delsoto, F.G. Battisti, A.K. da Silva, Dynamic modeling and control of a solar-powered Brayton cycle using supercritical CO2 and optimization of its thermal energy storage, Renew. Energy 206 (2023) 336–356, https://doi.org/10.1016/j.renene.2023.01.088.
[22] A. Saravanan, P. R. Yaashikaa, P. Senthil Kumar, A. S. Vickram, S. Karishma, R. Kamalesh, and Gayathri Rangasamy, "Techno-economic and environmental sustainability prospects on biochemical conversion of agricultural and algal biomass to biofuels, J. Clean. Prod. 414 (2023) 137749, doi: 10.1016/j.jclepro.2023.137749.
[23] A. Kumar, E. Singh, R. Mishra, S.L. Lo, S. Kumar, Global trends in municipal solid waste treatment technologies through the lens of sustainable energy development opportunity, Energy 275 (2023), 127471, https://doi.org/10.1016/j.energy.2023.127471.
[24] R. Singh, R.P. Singh, R. Singh, Biogas driven multigeneration integrated with simultaneous charging-discharging type thermal energy storage system, Energy Convers. Manag. 270 (2022), 116234, https://doi.org/10.1016/j.enconman.2022.116234.
[25] I. Dincer, Thermodynamics: A Smart Approach, John Wiley & Sons, 2020.
[26] R. Rivero, M. Garfias, Standard chemical exergy of elements updated, Energy 31 (15) (2006) 3310–3326, https://doi.org/10.1016/j.energy.2006.03.020.
[27] H. Zhang, X. Pan, J. Chen, J. Xie, Energy, exergy, economic and environmental analyses of a cascade absorption-compression refrigeration system using two-stage compression with complete intercooling, Appl. Therm. Eng. 225 (2023), 120185, https://doi.org/10.1016/j.applthermaleng.2023.120185.
[28] S. Samanta, D. Roy, S. Roy, A. Smallbone, A.P. Roskilly, Techno-economic analysis of a fuel-cell driven integrated energy hub for decarbonising transportation, Renew. Sustain. Energy Rev. 179 (2023), 113278, https://doi.org/10.1016/j.rser.2023.113278.
[29] S. Yu, Y. Fan, Z. Shi, J. Li, X. Zhao, T. Zhang, and Z. Chang, "Hydrogen-based combined heat and power systems: a review of technologies and challenges, Int. J. Hydrogen Energy 2023, doi: 10.1016/j.ijhydene.2023.05.187.
[30] M.H. Elbassoussi, M.A. Antar, S.M. Zubair, Hybridization of a triple-effect absorption heat pump with a humidification-dehumidification desalination unit: Thermodynamic and economic investigation, Energy Convers. Manag. 233 (2021), 113879, https://doi.org/10.1016/j.enconman.2021.113879.